Figure #	Figure title One sentence only	Filename This should be the name the file is saved as when it is uploaded to our system. Please include the file extension. i.e.: *Smith_ED Fig1.jpg*	Figure Legend If you are citing a reference for the first time in these legends, please include all new references in the Online Methods References section, and carry on the numbering from the main References section of the paper.
Extended Data Fig. 1	**Trabecular analysis method, example on *Pan troglodytes* metacarpus**.	ED_Fig1.jpg	a) An isosurface model of the metacarpus with inset parasagittal cross-section of the thumb metacarpal. b) 3D isosurface showing inner trabecular structure of the metacarpus. c) Segmented 2D cross-section of the thumb metacarpal (left), cortical and trabecular segmentation (centre), regular background grid overlaid on the isolated trabecular structure (right) and a close-up of this grid with a representation of the overlapping volumes of interest (VOIs) centred at each vertex of the background grid in purple (top). d) Interpolation of BV/TV values, measured in overlapping VOIs, onto 3D trabecular meshes. e) Anatomical landmarks (red), sliding semi-landmarks on curves (blue) and across the sub-articular surfaces (green) on the smoothed surface of the trabecular models. f) BV/TV values interpolated to each landmark and then divided by the mean value of each articular surface to produce RBV values on each landmark.
Extended Data Fig. 2	**Cross-sectional analysis method, example on a *Pongo* thumb metacarpal**.	ED_Fig2.jpg	a) A parasagittal cross-section image with its manual proximo-distal axis marked in blue and the computed eigenvector that best describes this axis marked in red. b) The 3D image is rotated by the angle between the two axes (green arrows). c) The cross-section of the rotated image shows the eigenvector now equals the proximo-distal axis of the bone and a 50% coronal cross-section, marked in orange, is orthogonal to the new axis. The position of this 50% diaphyseal mid-slice shown in 3D (d) and the anatomical axes used to calculate directional moments of inertia are

			radio-ulnar (RU), dorso-palmar (DP). The minimum (*Imin*) and maximum (*Imax*) moments of inertia calculated for this bone are depicted (f) and were averaged to generate the average area moment of inertia (*Iavg,* mm^4).
Extended Data Fig. 3	**Extant species average distributions of subchondral RBV across the metacarpus.**	ED_Fig3.jpg	a) distal, b) palmar and c) dorsal views. In addition, d) depicts the average distributions of RBV across the thumb metacarpal (Mc1) base (partially modified from[46,51]).
Extended Data Fig. 4	**Distributions of RBV across fossil hominin metacarpi.**	ED_Fig4.jpg	a) distal, b) palmar and c) dorsal views. Also, d) depicts the average distributions of RBV across the thumb metacarpal (Mc1) base and e) displays distal, palmar, dorsal and proximal views of individual fossil thumb metacarpals.

1

Item	Present?	Filename This should be the name the file is saved as when it is uploaded to our system, and should include the file extension. The extension must be .pdf	A brief, numerical description of file contents. i.e.: *Supplementary Figures 1-4, Supplementary Discussion, and Supplementary Tables 1-4.*
Supplementary Information	Yes	Supp_Info.pdf	Supplementary Tables 1-7 & Reference list
Reporting Summary	Yes	nr-editorial-policy-checklist_26_03_20.pdf	

2

3

Type	Number If there are multiple files of the same type this should be the numerical indicator. i.e.	Filename This should be the name the file is saved as when it is uploaded to our system, and should include the file extension. i.e.: *Smith_ Supplementary Video 1.mov*	Legend or Descriptive Caption Describe the contents of the file

	"1" for Video 1, "2" for Video 2, etc.		
Supplementary Software	1	Supplementary_software_1.html	An interactive 3D PCA depicting subchondral RBV variation across the finger metacarpals (Mc2-5). Each point represents the pattern of RBV across an associated metacarpus in one individual. Fossils are plotted in black and labeled.
Supplementary Software	2	Supplementary_software_2.html	An interactive 3D PCA depicting subchondral RBV variation across both subchondral surfaces on thumb metacarpals (Mc1). Each point represents the pattern of RBV across both subchondral surfaces in one individual. Fossils are plotted in black and labeled.
Supplementary Software	3	Supplementary_software_3.html	An interactive 3D PCA depicting subchondral RBV variation across the finger metacarpals (Mc2-4). Each point represents the pattern of RBV across an associated metacarpus in one individual. Fossils are plotted in black and labeled.
Supplementary Software	4	Supplementary_software_4.html	An interactive 3D PCA depicting subchondral RBV variation across the finger metacarpals (Mc2, 3 and 5). Each point represents the pattern of RBV across an associated metacarpus in one individual. Fossils are plotted in black and

			labeled.

The position of *Australopithecus sediba* within fossil hominin hand use diversity

Christopher J. Dunmore [1*], Matthew M. Skinner[1,2,3], Ameline Bardo [1], Lee R. Berger[3], Jean-Jacques Hublin[2], Dieter H. Pahr [4], Antonio Rosas[5], Nicholas B. Stephens[6] & Tracy L. Kivell [1,2,3]

[1]Skeletal Biology Research Centre, School of Anthropology and Conservation, University of Kent, Canterbury, UK
[2]Department of Human Evolution, Max Planck Institute for Evolutionary Anthropology, Leipzig, Germany
[3] Evolutionary Studies Institute, University of the Witwatersrand, Johannesburg, South Africa
[4] TU Wien Institute of Lightweight Design and Structural Biomechanics, Vienna, Austria
[5] Department of Paleobiology National Museum of Natural Sciences, CSIC, Madrid Spain
[6]Department of Anthropology, The Pennsylvania State University, Pennsylvania, USA
*Corresponding Author

Abstract

The human lineage is marked by a transition in hand use, from locomotion towards increasingly dexterous manipulation, concomitant with bipedalism. The forceful precision grips used by modern humans likely evolved in the context of tool manufacture and use, but when and how many times hominin hands became principally manipulative remains unresolved. We analyse metacarpal trabecular and cortical bone, which provide insight into behaviour during an individual's life, to demonstrate previously unrecognized diversity in hominin hand use. The metacarpals of the palm in *Australopithecus sediba* have trabecular morphology most similar to orangutans, and consistent with locomotor power grasping with the fingers, while that of the thumb is consistent with human-like manipulation. This internal morphology is the first record of behaviour consistent with a hominin that used its hand for both arboreal locomotion and human-like manipulation. This hand use is distinct from other fossil hominins in this study, including *Australopithecus afarensis* and *Australopithecus africanus.*

The dexterous modern human hand is often contrasted with the hands of other apes, which are integral to their arboreal and terrestrial locomotion [1,2,3]. The long thumb relative to the fingers[4], strong thenar musculature[5], reoriented radial carpals, and broad phalangeal apical tufts, that characterise the human hand[2] are thought to facilitate habitual forceful precision grips, power 'squeeze' grips and precision in-hand manipulation[6,7] unique to our species. The evolution of this dexterity is challenging to infer in Plio-Pleistocene hominins, including *Australopithecus*, *Paranthropus* and early *Homo*, since only indirect association exists between fossil specimens and archaeology evidencing this behaviour. Anatomical correlates of this dexterity often co-occur with ape-like features associated with arboreal locomotion, such as curved phalanges with well-developed flexor sheath ridges[8,9]. This mosaic of ape-like and human-like manual features is replicated in other postcranial elements of *Australopithecus afarensis* and *Australopithecus africanus*[10,11]. There is consensus that human-like features of the lower limb indicate at least

46 facultative terrestrial bipedality in *Australopithecus* (reviewed in[11]). However, the significance of
47 ape-like upper limb features has been debated, with some interpreting them as incidental retentions
48 from a more arboreal ancestor[12] while others consider these features as evidence of sustained
49 selection for arboreal locomotion[13]. These differing interpretations imply that either our
50 manipulative abilities began to evolve in hands freed of the demands of locomotion, or in an
51 arboreal hominin(s) that was not yet an obligate biped.

52 The mosaic *Australopithecus sediba* partial skeleton, Malapa Hominin 2 (MH2), offers a unique
53 Pleistocene perspective on the debate concerning locomotion in *Australopithecus*[14]. At 1.98 million
54 years old[15], MH2 lived just after the earliest lithic technology yet found in South Africa[16] (2.18 Million
55 years ago [Mya]) and after the earliest evidence of this technology in East Africa[17] (3.3 Mya).
56 Features of the lower limb and pelvis indicate straight-legged bipedalism in this species, perhaps
57 with a uniquely hyperpronated foot[18]. In contrast, MH2 has a relatively long upper limb and a
58 superiorly-oriented glenoid fossa of the scapula, as in other australopiths, which could be
59 interpreted as primitive retentions or functionally-significant arboreal adaptations[19]. Similarly, a
60 human-like thumb-to-finger length ratio suggests a manipulative hand in *A. sediba*, but this is
61 concomitant with moderately curved phalanges and well-developed flexor sheath ridges, considered
62 useful during arboreal locomotion[3]. Stable-carbon isotope, dental calculus and micro-wear analyses
63 all indicate this species was distinct among South African hominins in having a predominantly C_3 diet,
64 similar to savannah chimpanzees that mainly consume arboreal foods[20]. Therefore, as with other
65 *Australopithecus* species, the ape-like features of the MH2 hand may be interpreted as primitive
66 retentions, in the context of contemporaneous South African lithic evidence for forceful precision
67 grips, or indicative of a significant arboreal component in this species' locomotor repertoire and diet.
68 As behaviour changes faster than external morphology, this fossil evidence cannot discriminate
69 between these interpretations. To resolve this debate, we analyse morphology that can reflect
70 behaviour of fossil individuals during their lifetime.

71 Internal bone structure, including cortical bone distribution and trabecular architecture, can support
72 and refine interpretations of locomotor and manipulative behaviours, based on analyses of external
73 bone shape. Trabecular structure has been experimentally shown to (re)model in response to load
74 via bone functional adaptation[21] across a range of phylogenetically-distant taxa[22,23,24]. Comparative
75 studies have shown an association between trabecular structure and inferred habitual hand posture
76 in apes[24,25,26]. Trabecular bone of long bone epiphyses is deposited in response to habitual loading
77 from an adjacent joint, with deposition occurring along the direction of loading, to more efficiently
78 transfer force into the cortical diaphysis[27]. Diaphyseal and subchondral cortical bone has also been
79 shown to respond to habitual loading in a variety of mammals and birds[21,28,29]. Subchondral cortical
80 bone distribution and diaphyseal cross-sectional geometry have been demonstrated to correlate
81 with different locomotor modes in primate forelimbs and hands[30,31]. Habitual locomotor modes are
82 thought to produce strains that stimulate the formation of bone, which changes long bone cross-
83 sectional shape and robusticity[21]. The evidence of functional adaptation in cortical and trabecular
84 bone during the life of an individual, can provide critical information for reconstructing behaviour in
85 the past.

86 We analyse the relative cortical structure of metacarpal diaphyses and, for the first time, quantify
87 the subchondral trabecular bone volume fraction across the metacarpal heads and thumb
88 metacarpal base in great apes, humans and fossil hominins, using a novel geometric morphometric

approach. As there is substantial variation in systemic bone volume fraction across species, and its distribution throughout a joint is more informative for inferring habitually-loaded hand postures, we standardised bone volume fraction values for each subchondral metacarpal surface to calculate relative bone volume fraction (RBV) values. Initially, we assess whether these internal structures correlate with the presumed habitual hand postures employed by great apes during locomotion and manipulation. We expect the hyper-extension of metacarpophalangeal joints during knuckle-walking[32] will result in a dorsal concentration of RBV in the finger metacarpals of African great apes (*Pan paniscus, Pan troglodytes* and *Gorilla gorilla*). The flexion of these joints, when grasping branches in primarily arboreal orangutans (*Pongo* sp.)[33] is predicted to result in a palmar concentration of RBV in the finger metacarpals, whereas the flexion employed in recent human (*H. sapiens*) manipulation[34] is predicted to concentrate RBV more palmarly with increasingly ulnar rays[26]. In the metacarpophalangeal and trapeziometacarpal joints of the human thumb, we expect a concentration of radio-palmar RBV, reflecting an abducted opposed thumb, during habitual forceful precision grips[26,35]. The flexion and adduction of the thumb, during frequent pad-to-side grips, in other great apes is predicted to produce ulnar RBV concentrations at the metacarpophalangeal, and palmar RBV concentrations at the trapeziometacarpal joint[36,37,38]. We use this comparative context to infer habitual hand postures during manipulation in fossil *Homo sapiens* and *Homo neanderthalensis*, which are both considered to have modern human-like dexterity[39]. Finally, we infer hand use in Plio-Pleistocene hominins, including *A. afarensis, A. africanus, A. sediba* and SK 84, attributed to either *Paranthropus* or early *Homo*. We test if ape-like traits in the external morphology of Plio-Pleistocene hominins and, in particular, the associated hand of *A. sediba* MH2, were functionally significant or incidental traits from a more arboreal ancestor.

Metacarpals in extant great apes

We test the hypothesis that distribution of RBV would be consistent with metacarpophalangeal and trapeziometacarpal joint positions thought to be habitually loaded in great ape locomotion and manipulation. Higher average RBV in each species corresponds with predicted habitual metacarpal joint positions. Higher dorsal RBV in *Gorilla* (Fig. 1a) and *Pan* is consistent with the hyperextended metacarpophalangeal joints during knuckle-walking[32] (Extended Data 3). A principal components analysis (PCA) of subchondral RBV distribution in second to fifth metacarpal heads (Mc2-Mc5; Fig. 2a), the finger metacarpals, demonstrates that chimpanzees and bonobos, that share similar locomotor repertoires[40] and assumed habitual hand postures, are statistically indistinct. This PCA also distinguishes knuckle-walking African apes from *Pongo* and *Homo* (Fig. 2a; S 3). Higher palmar RBV in the finger metacarpals of *Pongo* (Fig. 1b) is consistent with habitually-flexed finger joints employed in arboreal power grasps, such as a 'double-locked' grip[33].Recent humans also show high palmar RBV, but this distribution is asymmetrical, showing increasing palmar RBV from Mc2 to Mc5, which is consistent with the simultaneous flexion and ulnar deviation of the finger joints when opposing the thumb during manipulation[34] (Fig. 1c).

In the first, or thumb, metacarpal (Mc1), recent humans display a statistically distinct pattern of RBV compared to great apes (Figs. 1c and 3; S3; Extended Data 4). This distribution of higher RBV in the radial region of the Mc1 head (distal) and radio-palmar region of the base (proximal) is compatible with thumb abduction, flexion and opposition during forceful precision grips, and in-hand manipulation[26,35]. Conversely, the great ape pattern shows higher average RBV values on the opposite side (disto-ulnar) of the Mc1 head and at the palmar Mc1 base, which is consistent with

thumb flexion and adduction (Fig. 1b) during 'pad-to-side' grips frequently practised by wild and captive great apes[36,37,38]. *Gorilla* shows a more pronounced pattern of the great ape RBV value distribution, which is significantly different from *Pan* species (S.3).

To assess the biomechanical importance of the thumb in each species we investigate bending stiffness and shape of the metacarpal diaphysis, at 50% bone length, across all the metacarpals. We predicted, due to higher radio-ulnar loading of the muscular thumb in recent human manipulation[2,5], the thumb metacarpal diaphysis would be radio-ulnarly wider and possess higher bending stiffness relative to the finger metacarpals. In extant apes, we predicted bending stiffness would be similar in the thumb and finger metacarpals, as it appears to be less frequently forcefully loaded compared to humans[36,37,38]. Results show that human thumb metacarpals have a significantly higher average area moment of inertia (measuring bending stiffness) than extant great apes (S5, Fig. 4). However, although human thumb metacarpal midshafts are consistently radio-ulnarly wider than those of the finger metacarpals, this ratio is not significantly different from most great apes, in which it is highly variable intraspecifically (S5, Fig. 4).

Metacarpal internal trabecular and cortical bone structure clearly distinguish recent humans from extant great apes. In humans, this internal structure reflects primarily manipulative fingers and a strong thumb. In great apes it reflects reduced biomechanical importance of the thumb, and fingers that are principally loaded during locomotion, including grasping branches, knuckle-walking, or both.

Hand use in fossil Homo

The fossil *H. sapiens* (Ohalo II H2, Arene Candide 2 and Barma Grande 2) RBV distribution places them near, or within, the recent human range across the metacarpals (Figs. 2 and 3). Fossil *H. sapiens* cortical bone exhibits the same shape ratio but a stiffer Mc1 diaphysis than in recent humans. In contrast, *H. neanderthalensis* specimens (Kebara 2, El Sidrón, Tabun C1) have a similar diaphyseal bending stiffness of the thumb metacarpal, relative to the finger metacarpals, but a radio-ulnarly narrower thumb metacarpal midshaft, compared to recent humans (Fig. 4). The finger metacarpal RBV distribution in both *H. neanderthalensis* specimens is separated from recent and fossil *H. sapiens* by higher values on the distal aspect of the metacarpus, especially in the more ulnar rays. The RBV distribution of the *H. neanderthalensis* thumb metacarpal is variable; Feldhofer 1 clusters with *H. sapiens* while Kebara 2 and El Sidrón have higher values toward the ulnar aspect of the Mc1 head, which is more similar to the pattern found in *Pan* (although only Kebara 2 falls close to the *Pan* distribution; Fig. 3). While implying different habitually-loaded hand postures from recent humans, this thumb metacarpal signal is still consistent with manipulation.

Hand use in Plio-Pleistocene hominins

There is no complete associated metacarpus for *A. africanus* or *A. afarensis*, but a partial composite metacarpus can be created for each species (see Methods). Although drawn from different sub-sets of the data, the trabecular distribution within both the *A. africanus* Mc2-4 (Fig. 2b) and *A. afarensis* Mc2, 3 and 5 (Fig. 2c) is intermediate between all extant taxa. SK 84 is an Mc1 attributed to *Paranthropus* or early *Homo*[41] and has a RBV pattern that is most similar to that of extant great apes (Fig. 3). The *A. africanus* thumb metacarpal (StW 418) clusters near those of *H. neanderthalensis* (Fig. 3) but displays a distinct pattern of RBV values unlike any *Homo* specimen studied. The relative

bending stiffness of StW 418 is also significantly lower than that of recent humans, falling within the range of extant apes (Fig. 4).

The finger metacarpals of *A. sediba* demonstrate a different RBV distribution from other australopiths, consistently falling at the edge of the *Pongo* range (Figs. 2a, b, c). In stark contrast, the associated thumb metacarpal has a trabecular structure that falls within the range of recent humans and *Gorilla*, due to one specimen that extended the latter species' range (Fig. 3). However, the Mc1 trabecular structure in *A. sediba* is closest to the human average and, indeed, overlaps with one recent human specimen, itself not an outlier of the human range (Fig. 3,S4). The relative bending stiffness of the *A. sediba* thumb metacarpal, uniquely falls between extant great apes and recent humans, though the midshaft of the thumb has a shape similar to the latter (Fig. 4). These results suggest the *A. sediba* hand experienced a predominant loading regime not seen in any extant great ape, recent human or other fossil hominin examined in this study. They are also the first direct record of *in vivo*, arboreal grasping and human-like manipulation combined in a complete and associated hominin hand.

Discussion

Cortical and trabecular metacarpal structure, clearly distinguishes presumed habitual hand loading patterns across humans and great apes, even though the interplay between load magnitude and frequency, as well as several other factors, including genetics, hormones, or systemic patterns, in shaping internal bone structure is not fully understood[21,28,42]. The current trabecular data are consistent with fingers that are hyper-extended during African ape knuckle-walking and fingers that are habitually flexed during arboreal power grasping in *Pongo*. The *H. sapiens* trabecular distribution is consistent with flexed, ulnarly deviated fingers and an opposed thumb during manipulation, an interpretation supported by a thumb midshaft that is more resistant to bending (stiffer), relative to those of the finger metacarpals, than in great apes. This functional signal among extant taxa, combined with a growing body of comparative and experimental studies demonstrating bone functional adaptation[21,22,23,24,25], allows us to reconstruct key aspects of hand loading in fossil hominins.

Fossil *H. sapiens* demonstrated a pattern of internal bone structure similar to that of recent humans, but had higher relative diaphyseal bending stiffness in the thumb. This disparity may reflect greater loading of the thumb in fossil *H. sapiens* or a systemic reduction of bone robusticity known to have occurred in Neolithic humans[43]. The internal bone structure of *H. neanderthalensis* was consistent with habitually less-flexed fingers and a more adducted thumb, than in recent and fossil humans. While these joint positions are also habitually used by great apes, *H. neanderthalensis* external morphology is broadly similar to that of recent humans. The subtle differences from humans in *H. neanderthalensis* external metacarpal morphology, including less radio-ulnarly asymmetric second and fifth metacarpal heads, would restrict the axial rotation of the fingers during flexion in precision grips[39]. Combined with a capitate possessing a more parasagittal orientation of the second metacarpal facet and a radio-ulnarly flatter fifth metacarpal base than in humans, this Neanderthal morphology has been interpreted as better adapted to axial loads, which is consistent with a more distally loaded metacarpophalangeal joint[39]. This suggests that this species may have adopted grips favouring less flexed fingers and a somewhat adducted thumb, similar to the human power 'squeeze' grip and 'pad-to-side' precision grip[39]. Such grips may have been frequently employed to

grip hafted tools or to secure scrapers, respectively. These tool technologies are commonly associated with *H. neanderthalensis* in the archaeological record[39]. The diversity of lithic tools produced by this species[44], as well as morphological evidence for a distinction between northern and southern European *H. neanderthalensis*[45], likely explains why the trabecular structure of the thumb metacarpal of Feldhofer 1 is more similar to recent humans than other *H. neanderthalensis.*

Variation in the thumb trabecular distributions, across australopiths and Swartkrans specimen SK 84 is reinforced by the trabecular patterns of the australopith finger metacarpals. Although diversity may be expected in taxa that occupy large geographical and temporal ranges, *A. afarensis, A. africanus* and *A. sediba* all share relatively gracile metacarpal morphology, moderately curved phalanges, and similar (estimated) hand proportions, which would not necessarily imply such variation in metacarpal loading. While caution is warranted when interpreting small fossil sample sizes, the SK 84 thumb metacarpal shows a more robust *Homo*-like external morphology, but it is the only fossil specimen to fall within the great ape trabecular distribution (Fig. 3). The relative bending stiffness of the thumb metacarpal in *A. africanus* similarly appears ape-like. Although the lack of an *A. afarensis* or *A. africanus* associated metacarpus makes comparisons challenging, *A. sediba* loaded its hand distinctly differently. The internal bone structure of the *A. sediba* MH2 hand has a uniquely mosaic functional signal in our fossil sample. The trabecular distribution within the finger metacarpal heads suggests *A. sediba* loaded its finger joints in a flexed power grip posture, similar to that of *Pongo.* In contrast, the internal structure of the thumb metacarpal is human-like, otherwise only showing an affinity with one *Gorilla* specimen, a dexterous taxon[38,46] which has the closest thumb-to-finger length ratio to humans among great apes[4]. This trabecular distribution in MH2 suggests habitual use of an abducted opposed thumb that is typical of human forceful precision grips. While human manipulation also requires flexed fingers, it loads the metacarpal heads differently than locomotor power grasping, as demonstrated in the trabecular separation of later *Homo* (*H. sapiens* and *H. neanderthalensis*) and *Pongo* (Fig .2, S3). Therefore, the trabecular structure of the MH2 finger metacarpals is interpreted as reflecting locomotor, rather than manipulative, grasping. The palaeoenvironment of Malapa would have offered opportunities for flexed-finger rock climbing which may also be compatible with this trabecular evidence. However, as the best extant analogue for the trabecular pattern found in the *A. sediba* palm is that of the mostly arboreal orangutan, it is more conservative to interpret the MH2 pattern as reflecting locomotor grasping in an arboreal context.

This trabecular evidence for great ape-like arboreal power grasping in the fingers and human-like manipulation in the thumb of *A. sediba* is present within a thumb metacarpal that is cortically more robust than its finger metacarpals, but intermediate between great apes and humans (Fig. 4). The external morphology of the *A. sediba* thumb is also mosaic, with a longer thumb relative to the fingers than even that of recent humans, suggesting enhanced opposability to the fingers, but this thumb is remarkably gracile with poorly developed entheses, suggesting a limited degree of force production[3, 7]. The finger metacarpals appear gracile but with uniquely large proximal bases and distal heads[47]. Unlike humans, however, the Mc4 and Mc5 are more robust than the Mc2 and Mc3 in *A. sediba*[47], a *Pongo*-like pattern, thought to reflect more uniform use of digits in arboreal grasping[29,33]. The moderately curved phalanges and well-developed flexor sheath ridges on the proximal and intermediate phalanges in *A. sediba* have been interpreted as evidence of arboreal climbing[3,47]. Similar morphology in *A. afarensis* has been functionally interpreted in this way[13], although others have disagreed[12]. The finger metacarpal trabecular structure demonstrates that

these arboreal features are functionally significant and that *A. sediba* was using flexed, grasping postures similar to those used by *Pongo* in an arboreal environment. While it must be remembered the MH2 hand represents a single adult, it suggests that the arboreal features that characterise the *A. sediba* upper limb are also adaptive, although further internal bone analysis of the postcrania would help to confirm this.

Our internal bone results provide the first evidence supporting the use of ape-like features within the *A. sediba* hand*,* and do not support their interpretation as incidental retentions from a more arboreal ancestor. This record of *in vivo* manual behaviour reveals that while the hand of the terrestrially bipedal *A. sediba* was used for manipulation, it was also used for arboreal power grasping, possibly to access arboreal food sources. Our analysis suggests *A. afarensis* and *A. africanus* were using their hands in a different manner to that of *A. sediba*, which may not be surprising given variation in australopith postcranial morphology, particularly the derived *A. afarensis* foot[48]. However, complete and associated hands of other hominins are required to infer hand use with the same resolution that we can for *A. sediba*. We do not mean to imply that *A. afarensis* or *A. africanus* were not arboreal, but that, if they were, they were likely using their hands in a different manner than *A. sediba* did. Just as we do not know which of these hominin species made stone tools, we are as yet, equally unaware of precisely how far each species adopted obligate bipedalism, or if they did so in similar ways. *A. sediba* likely reflects one of many transitions to obligate bipedalism in Plio-Pleistocene hominins, one in which *A. sediba* used its hand both for manipulation and arboreal locomotion in a distinct manner.

Methods

Scanned samples and Image segmentation

Extant specimens were micro-CT scanned with a BIR ACTIS 225/300, Diondo D3, or Skyscan 1172 high resolution microCT scanners at the Department of Human Evolution, Max Planck Institute for Evolutionary Anthropology, Germany, or with the Nikon 225/XTH scanner at the Cambridge Biotomography Centre, University of Cambridge, UK. Fossils were scanned at these or their host institutions. Scans were performed at 100-160kV and 100-140µA, using a brass or copper filter of 0.25-0.5mm. The scans were reconstructed to create volumetric images with an isometric voxel size between 13-57µm, depending on the size of the specimen.

If the quality of micro-CT reconstructed volume, as well as the trabecular and cortical preservation, were appropriate for at least one of the analyses, the metacarpal image was cropped and reoriented into standard anatomical positions (Extended Data 1a, inset), and unwanted dense inclusions that would be erroneously classified as bone were removed in Avizo 6.3 (Visualization Sciences Group, SAS). The Ray Casting Algorithm[49] was used to segment bone from other materials in bone metacarpals, while the MIA-Clustering method[50] (Extended Data 1b, c) was used to segment fossils due to the frequent presence of introgressive material.

Trabecular analysis

Segmented metacarpal images were processed with the whole-epiphysis method, as described in more detail in many studies[24,26,42]and subsequent geometric morphometric landmark analysis was performed in a similar manner to that described in[46,51]. In brief, a number of image filters, run via medtool 4.2 (Dr. Pahr Ingenieurs e.U.), automatically isolated first the whole bone followed by a

separation of inner trabecular structure from the cortical bone. The whole bone is segmented by a "fill" operation i.e. casting rays from the outer cortical shell at multiple angles followed by a morphological closing. This whole bone volume is eroded by a region growing in combination with morphological operations. Thus, the inner trabecular volume as well as the cortical shell of the metacarpal is obtained. A structured background grid of 2.5mm cubes was superimposed on the isolated trabecular volume and overlapping spherical volumes of interest (VOI), 5 mm in diameter, were centred at each of its vertices (Extended Data1c). Trabecular bone volume fraction (BV/TV) was then measured in each VOI and the values were interpolated on the centroids of a 3D tetrahedral mesh of the trabecular volume, created with CGAL (Extended Data 1d). BV/TV is strongly associated with the mechanical properties of trabecular bone (as referenced in [25,26]) and is not markedly allometric[53].

The present study focuses on subchondral or subarticular BV/TV since forces at a joint must pass through part of the subchondral cortical bone[29,30] and trabecular structure, before reaching the deep trabecular structure or diaphyseal cortical bone[27]. Therefore, if bone functional adaption to habitually loaded joint positions exists, it should be found in the subchondral trabeculae[46,51]. To achieve this subchondral trabecular analysis the outer surface of the 3D trabecular mesh was isolated in Paraview and a Poisson surface reconstruction filter was used to smooth the surface in Meshlab. Metacarpal surfaces from left hands were then mirrored so that they were oriented in the same manner as those from right hands, for homologous functional comparison. Surfaces of all metacarpal heads and thumb metacarpal bases were manually landmarked in Checkpoint (Stratovan Corporation, Davis, CA). Anatomical landmarks used here have been previously shown to be repeatable and are listed in previous work[46,51]. A template of landmarks was manually created on a randomly chosen specimen for finger metacarpal (Mc2-5) heads, thumb (Mc1) metacarpal heads and thumb metacarpal bases, respectively in Avizo 6.3 (Visualization Sciences Group, Germany), following[46,51]. The sliding semi-landmarks that bordered, and those that were equally distributed over, the sub-articular surface of each template were then projected onto the appropriate surface of each metacarpal in the sample via the Morpho package in R. This package was also used to relax projected landmarks onto each metacarpal surface by minimising bending energy and to slide the semi-landmarks along their respective curves and over the surface by minimising Procrustes distances (Extended Data 1e). In order to interpolate BV/TV to these landmarks a custom Python script was used to assign BV/TV values of each tetrahedra in the unsmoothed trabecular mesh created in medtool 4.2 to the centre of their surface triangles. The Python module SciPy was used to interpolate these centre BV/TV values to the closest (nearest-neighbour) landmark on the smooth surface (Extended Data 1f). In R, a generalised Procrustes procedure was run on these landmarks using the Geomorph package to create 204 sets of 173 homologous finger metacarpal head 3D landmarks and 58 sets of both 49 thumb metacarpal head, and 40 thumb metacarpal base, 3D homologous landmarks, all with an associated BV/TV value. As the raw BV/TV values may incorporate both biomechanically functional and systemic differences between species or individuals[42], we follow other studies that standardise BV/TV in order to analyse the distribution, rather than raw magnitude, of trabecular volume beneath joint surfaces[4246,51]. Briefly, at least one of these species, humans, is known to have systemically lower BV/TV than the others[42,43,]. Therefore comparisons of highest BV/TV values on a given region of a human subchondral surface, with the lowest of those on the same region of another species' subchondral surface, may yield no significant statistical difference, because this difference in magnitude obscures the difference in distribution[46,51 52]. Therefore, the BV/TV value at each landmark on a subchondral surface was divided by the

arithmetic mean of all landmark BV/TV values on that subchondral surface of that specimen, to derive a relative measure of bone volume fraction (RBV). While this standardisation approach does not consider some important information contained in BV/TV, such as difference in overall bone volume magnitude, it does allow for the analyses of different patterns of bone volume distribution. RBV values approaching one indicate BV/TV values close to the average BV/TV of that subchondral surface.

Cross-sectional geometry

Several palaeoanthroplogical and bio-archaeological studies have employed cross-sectional geometry (CSG) at the mid-diaphysis of long bones to investigate cortical bone functional adaptation[21,31]. Though findings have cautioned against a simple interpretation of comparative results[28], several experimental studies have shown that loading regime does affect the cross-sectional properties of cortical bone (as reviewed in[21]).

In order to generate a 50% mid-diaphysis axial cross-section, a 2D sagittal cross-section of each segmented metacarpal image was created using medtool 4.2. A homologous axial cross-section requires a mid-slice orthogonal to the long axis of the metacarpal, however several specimens studied, particularly those of *Pongo*, were curved, resulting in an oblique axial cross-section in an anatomical position that is not homologous to those of straighter metacarpals. In order to ameliorate the effect of metacarpal curvature on axial cross-section homology, the Numpy Python module was used to run a PCA on the 2D co-ordinates of bone pixels in the sagittal cross-section image (Extended Data 2a). The largest eigenvector generated by this PCA linearly describes the variance in the position of the pixels that form the bone image (e.g. the grey pixels in Extended Data 2a.). This eigenvector is then a straight line, which better describes the long axis of the metacarpal than the initial long axis found in an anatomical position, as it incorporates the relative amount of curvature in each bone. The angle between the eigenvector and the y-axis was found and the segmented 3D volume was then rotated by this angle in the sagittal plane using medtool 4.2 (Extended Data 2b). ImageJ was then used to find the most proximal and distal bone pixel in the rotated sagittal image and the midpoint between them in the y-axis (Extended Data 2c). Medtool 4.2 was used to extract a homologous axial 50% mid-slice from each rotated 3D segmented volume in the entire sample (Extended Data 2d).

The Slice Geometry function of BoneJ was run on these homologous axial mid-slices to calculate the maximum (*Imax*) and minimum (*Imin*) area moments of inertia (second moments of area) as well as the area moment of inertia in the dorso-palmar (*IDP*) and radio-ulnar (*IRU*) planes in each case (Extended Data 2e, f). The average of *Imax* and *Imin (Iavg),* was used as a measure of overall diaphyseal bending stiffness as it is directly proportional to the average bending rigidity of a bone[54]. These measures were calculated in mm^4 and a species mean for each metacarpal is reported in S6. The ratio of *IDP/ IRU* measures how a bone can resist bending forces in each anatomical plane, with ratios above one indicating a more dorso-palmar bending stiffness, ratios below one indicating more radio-ulnar resistance, and ratios around one indicating similar resistance in both planes. Both *Iavg* and *IDP/ IRU* of the thumb metacarpal (Mc1) were divided by the arithmetic mean *Iavg* and *IDP/ IRU* of the finger metacarpals (Mc2-5). The resulting ratios indicate the biomechanical bending stiffness at mid-diaphysis of the thumb metacarpal relative to the rest of the metacarpus and how far the direction of this resistance to bending departs from the finger metacarpals.

Statistical analysis

In order to analyse the distribution of subchondral RBV, the mean values of each landmark per species were visualised on canonical metacarpal surfaces created using a statistical shape model in wxRegSurf (http://mi.eng.cam.ac.uk/~ahg/wxRegSurf/). For finger metacarpals (Mc2-5), each of the 692 landmark values were treated as variables in a principal components analysis (PCA). The first three principal components (PCs) comprised 54% of the variation and further PCs described less than 10% additional variation. Therefore, in order to test if overall RBV distribution was different between extant species, an omnibus and subsequent pairwise one-way permutational MANOVAs were run on the first three PC scores of each set of finger metacarpals, using the Vegan and RVAideMemoire packages in R. Before these tests were performed, a test of multivariate homogeneity of variance was performed on the Euclidean distance matrix that describes the PC scores and a Bonferroni correction was applied to all pairwise results, to ensure valid comparisons. A permutation approach was taken as not all data met the assumption of multivariate normality. This approach was separately applied to the subchondral RBV of the thumb metacarpal (Mc1), as this bone has two mobile joints that are loaded differently, and likely concomitantly, in different habitual thumb postures. For this analysis both proximal and distal epiphyses were combined in the same manner as the four finger metacarpal heads. RBV distribution of individual subchondral surfaces are visualised for fossils (Extended Data 4) and have been analysed separately for extant samples in previous work[46]. In order to determine if individual fossils were significantly different from extant groups a permutational, Hotelling's one-sample T^2 test was employed from the R Package Compositional for the Mc1 and Mc2-5 separately. While one-sample test results must be interpreted with caution, as their statistical power is limited, these tests provide some statistical interpretation of the results visualised in the PCAs until further fossils are discovered. To test for significant differences in the relative cortical bending stiffness and shape of metacarpal diaphyses between extant species, a Kruskal-Wallis with post-hoc Dunn's tests were run on *Iavg* and *IDP/ IML* ratios respectively, with a Bonferroni correction. A one-sample Wilcoxon signed rank test was used to determine if individual fossils were significantly different from extant species for each variable separately, though again these are interpreted with caution. All statistical tests were performed in R, with a p-value < 0.05 taken as significant.

Figure legends

Fig. 1. Average relative trabecular bone (RBV) distribution in great ape and human metacarpals during habitual hand postures. RBV is the ratio of subchondral trabecular bone to space at each landmark divided by the average values for all landmarks on that subchondral surface. Higher RBV indicates relatively more bone in this part of the metacarpal (red landmarks) while lower RBV indicate relatively less bone (blue landmarks). RBV values ~1 indicate trabecular bone is near the average of the surface in this area (white landmarks)**.** Hand postures are shown for (a) knuckle-walking in *Gorilla*, (b) arboreal locomotion in *Pongo* and (c) manipulation in humans. Though not habitually used by *Pongo* during arboreal locomotion, the arrow in (b) illustrates adduction of the thumb during 'pad-to-side' grips habitually used by all non-human apes and in (c) abduction of the 'pad-to-pad' opposed thumb in humans during precision grips. Species average RBV distribution in the Mc1 base is depicted inset for (b) and (c).

Fig. 2. Relative trabecular bone volume fraction (RBV) distribution in the metacarpal heads of the palm. a) A 3D PCA depicting subchondral RBV variation across the finger metacarpals (Mc2-5). Each

point represents the pattern of RBV across an associated metacarpus in one individual. Fossils are plotted in black and labelled. RBV distribution clearly distinguishes among the extant taxa, apart from both *Pan* species that have very similar locomotor repertoires. Both fossil *H. sapiens* (Ohalo II and Arene Candide 2) fall within the proximity of recent humans, while *H. neanderthalensis* specimens (Kebara 2 and El Sidrón) are separated from humans on PC3. *A. sediba* is distinct, situated closest to *Pongo* and far from humans and great apes. b) The same PCA but based on just Mc2-4 for comparison with *A. africanus* composite sample and c) based on Mc 2, 3 and 5, for comparison with *A. afarensis* composite sample. Though interpretation of incomplete and composite metacarpi must be undertaken with caution, note that in neither case do *A. afarensis* or *A. africanus* have a similar RBV distribution to that of *A. sediba*.

Fig. 3. Relative trabecular bone volume fraction (RBV) distribution in the thumb metacarpal. A 3D PCA depicting subchondral RBV variation across the thumb metacarpal (Mc1) head and base. Each point represents the pattern of RBV across both epiphyseal surfaces in one individual. Fossils are plotted in black and labelled. RBV clearly distinguishes modern humans from great apes and *Gorilla* somewhat departs from the great ape pattern. SK 84 (assigned to either *Homo* or *Paranthropus*), is situated within the great apes. All fossil *H. sapiens* (Arene Candide 2, Barma Grande 2 and Ohalo II) and Feldhofer 1 fall close to the recent human sample. Kebara 2, El Sidrón and StW 418 (an *A. africanus* specimen) are separated from all extant species. *A. sediba* falls within the range of recent humans.

Fig. 4. Relative cortical bending stiffness of thumb metacarpals at midshaft. A bivariate plot of cross-sectional geometry variables. For each hand, a ratio of the thumb metacarpal (Mc1) and the mean finger metacarpal (Mc2-5) average area moments of inertia (*Iavg,* mm^4) is plotted on the X-axis. The ratio of area moments of inertia (mm^4) in the dorso-palmar (DP) and radio-ulnar (RU) planes is a shape index for a metacarpal diaphysis. A ratio of these shape indices between the thumb metacarpal and average finger metacarpals is plotted on the y-axis. Representative metacarpi of *P. troglodytes* and *H. sapiens* are depicted adjacent to their values. Note the separation of recent and fossil humans from great apes and *A. africanus. A. sediba* is situated between recent humans and great apes.

Reference

[1] Susman, R. L. Fossil evidence for early hominid tool use. *Science* **265** 1570-1573 (1994).

[2] Tocheri, M. W., Orr, C. M., Jacofsky, M. C. & Marzke M. W. The evolutionary history of the hominin hand since the last common ancestor of *Pan* and *Homo*. *J. Anat.* **212**, 544-562 (2008).

[3] Kivell, T. L. , Kibii, J. M., Churchill, S. E., Schmid, P. & Berger, L. R. *Australopithecus sediba* hand demonstrates mosaic evolution of locomotor and manipulative abilities. *Science* **333**, 1411-1417 (2011).

[4] Almécija, S., Smaers, J. B. & Jungers, W. L. The evolution of human and ape hand proportions. *Nat. commun.* **6**, 7717 (2015).

[5] Marzke, M. W. et al. Chimpanzee thumb muscle cross sections, moment arms and potential

torques, and comparisons with humans. *Am. J. Phys. Anthropol.* **110**, 163-178 (1999).

[6] Marzke, M. W., Wullstein, K. L. & Viegas, S. F. Evolution of the power ("squeeze") grip and its morphological correlates in hominids. *Am. J. Phys. Anthropol.* **89**, 283-298 (1992).

[7] Christel, M. Grasping techniques and hand preferences in Hominoidea. in *Hands of Primates* (eds. Preuschoft, H. & Chivers, D.J.) 91-108 (Springer, Verlag, 1993).

[8] Bush, M. E., Lovejoy, C. O., Johanson D. C. & Coppens, Y. Hominid carpal, metacarpal, and phalangeal bones recovered from the Hadar Formation: 1974–1977 collections. *Am. J. Phys. Anthropol.* **57**, 651-677 (1982).

[9] Ricklan, D. E. Functional anatomy of the hand of *Australopithecus africanus. J. Hum. Evol.* **16**, 643-664 (1987).

[10] Green, D. J., Gordon, A. D. & Richmond, B. G. Limb-size proportions in *Australopithecus afarensis* and *Australopithecus africanus*. *J. Hum. Evol.* **52**, 187-200, (2007).

[11] Kimbel, W. H. & Delezene, L. K. "Lucy" redux: A review of research on *Australopithecus afarensis*. *Am. J. Phys. Anthropol.* **140**, 2-48 (2009).

[12] Latimer, B. Locomotor behaviour in *Australopithecus afarensis*: The issue of arboerality. in *Origine(s) de la Bipédie chez les Homindés* (eds. Coppens, Y. & Senut,B.) 169-176 (CNRS Cahiers de Paleoanthropologie, 1991)

[13] Stern, J. T., & Susman, R. L. The locomotor anatomy of *Australopithecus afarensis*. *Am. J. Phys. Anthropol.* **60**, 279-317 (1983).

[14] Berger, L. R., et al. *Australopithecus sediba*: A new species of *Homo*-like australopith from South Africa. *Science* **328**, 195-204 (2010).

[15] Pickering, R., et al. *Australopithecus sediba* at 1.977 Ma and implications for the origins of the genus *Homo*. *Science* **333**, 1421-1423, (2011).

[16] Granger, D. E. et al.,New cosmogenic burial ages for Sterkfontein Member 2 *Australopithecus* and Member 5 Oldowan. *Nature* **522**, 85-88 (2015).

[17] Harmand, S. et al. 3.3-million-year-old stone tools from Lomekwi 3, West Turkana, Kenya. *Nature* **521**, 310-315 (2015).

[18] DeSilva, J. M., et al. The lower limb and mechanics of walking in *Australopithecus sediba*. *Science* **340**, 1232999 (2013).

[19] Churchill, S. E., et al. The upper limb of *Australopithecus sediba*. *Science* **340**, 1233477 (2013).

[20] Henry, A. The diet of *Australopithecus sediba*. *Nature* **487**, 90-93 (2012).

[21] Ruff, C., Holt, B. & Trinkaus, E. Who's afraid of the big bad Wolff?:"Wolff's law" and bone functional adaptation. *Am. J. Phys. Anthropol.* **129**, 484-498 (2006).

[22] Biewener, A. A., Fazzalari, N. L., Konieczynski, D. D. & Baudinette, R. V. Adaptive changes in trabecular architecture in relation to functional strain patterns and disuse. *Bone* **19**, 1-8 (1996).

[23] Barak, M. M., Lieberman, D. E. & Hublin, J-J. A Wolff in sheep's clothing: trabecular bone adaptation in response to changes in joint loading orientation. *Bone,* **49**, 1141-1151 (2011).

[24] Tsegai, Z. J. et al. Trabecular bone structure correlates with hand posture and use in hominoids. *PLoS ONE* **8**, e78781 (2013).

[25] Barak, M. M., Sherratt, E. & Lieberman D.E. Using principal trabecular orientation to differentiate joint loading orientation in the 3rd metacarpal heads of humans and chimpanzees. *J. Hum. Evol.* **113**, 173-182 (2017).

[26] Stephens, N. B., Kivell, T. L., Pahr, D., Hublin, J-J. & Skinner, M. M. Trabecular bone patterning across the human hand. *J. Hum. Evol.* **123**, 1-23 (2018).

[27] Currey, J.D. *Bones: structure and mechanics.* (Princeton Univ. Press, Princeton, 2006)

[28] Wallace, I., Demes, B. & Judex, S. Ontogenetic and Genetic Influences on Bone's Responsiveness to Mechanical Signals. in *Building Bones: Bone Formation and Development in Anthropology* (eds. Percival, C.J. & Richtsmeier, J.T.) 233-253 (Cambridge Univ. Press, Cambridge, 2017).

[29] Patel, B. A., & Carlson, K. J. Apparent density patterns in subchondral bone of the sloth and anteater forelimb. *Biol Lett.* ***4***, 486-489 (2008).

[30] Carlson, K. J., & Patel, B. A. Habitual use of the primate forelimb is reflected in the material properties of subchondral bone in the distal radius. *J.Anat.* ***208***, 659-670 (2006).

[31] Marchi, D. The cross-sectional geometry of the hand and foot bones of the Hominoidea and its relationship to locomotor behavior. *J. Hum. Evol.* **49**, 743-761 (2005).

[32] Tuttle, R. H. Knuckle-walking and the evolution of hominoid hands. *Am. J. Phys. Anthropol.* **26**, 171-206 (1967).

[33] Rose, M. D. Functional anatomy of the cheiridia. in *Orangutan Biology*, (ed. Schwartz, J.) 299-310 (Oxford Univ. Press, Oxford, 1988)

[34] Napier, J. R. The prehensile movements of the human hand. *J. Bone. Joint. Surg. [Br].* **38**, 902-913 (1956).

[35] D'Agostino, P., Dourthe, B. , Kerkhof, F., Stockmans, F. & E. E. Vereecke. *In vivo* kinematics of the thumb during flexion and adduction motion: Evidence for a screw-home mechanism. *J. Orthop. Res.* **35**, 1556-1564 (2017).

[36] Marzke, M. W., Marchant, L. F., McGrew, W. C. & Reece, S. P. Grips and hand movements of chimpanzees during feeding in Mahale Mountains National Park, Tanzania. *Am. J. Phys. Anthropol.* **156**, 317-326 (2015).

[37] Bardo, A., Cornette, R., Borel A. & Pouydebat, E. Manual function and performance in humans, gorillas, and orangutans during the same tool use task. *Am. J. Phys. Anthropol.* **164**, 821-836 (2017).

[38] Neufuss, J., Robbins, M., Baeumer, J., Hulme, T. & Kivell T. L. Manual skills for food processing by mountain gorillas in Bwindi Impenetrable National Park, Uganda. *Biol. J. Linnean. Soc.* **127**, 543-562 (2018).

[39] Niewoehner, W. A., Neanderthal hands in their proper perspective. in *Neanderthals revisited: New approaches and perspectives* (eds. Harvati, K. & Harrison, T.) 157-190 (Springer Netherlands, 2006).

[40] Doran, D. M. Comparative locomotor behavior of chimpanzees and bonobos: the influence of morphology on locomotion. *Am. J. Phys. Anthropol.* **91**, 83-98 (1993).

[41] Trinkaus, E. & Long J. C. Species attribution of the Swartkrans Member 1 first metacarpals: SK 84 and SKX 5020. *Am. J. Phys. Anthropo.l* **83**, 419-424 (1990).

[42] Tsegai, Z. J., Skinner, M. M., Pahr, D. H., Hublin J- J. & Kivell T. L. Systemic patterns of trabecular bone across the human and chimpanzee skeleton. *J. Anat.* **232**, 1-16 (2018).

[43] Chirchir, H., et al. Recent origin of low trabecular bone density in modern humans. *PNAS* **112**, 336-371 (2015).

[44] Hardy, B. L., et al. Impossible Neanderthals? Making string, throwing projectiles and catching small game during Marine Isotope Stage 4 (Abri du Maras, France). *Quat. Sci. Rev.* **82**, 23-40 (2013).

[45] Rosas, A., et al. Paleobiology and comparative morphology of a late Neandertal sample from El Sidrón, Asturias, Spain. *PNAS* **103**, 19266-19271 (2006).

[46] Dunmore, C. J., Bardo, A., Skinner, M. M., & Kivell, T. L. Trabecular variation in the first metacarpal and manipulation in hominids. *Am. J. Phys. Anthropol.* **171**, 219-241 (2019).

[47] Kivell, T. L., Churchill, S., Kibii, J., Schmid P. & Berger, L. R. The Hand of *Australopithecus sediba*. *Paleo. Anthro.* 282-333 (doi:10.4207/PA.2018.ART115, 2018).

[48] Ward, C. V., Kimbel, W. H. & Johanson, D. C. Complete fourth metatarsal and arches in the foot of *Australopithecus afarensi*s. Science, **331**, 750-753 (2011).

[49] Scherf, H & Tilgner, R. A new high-resolution computed tomography (CT) segmentation method for trabecular bone architectural analysis *Am. J. Phys. Anthropol.* **140**, 39-51 (2009).

[50] Dunmore, C. J., Wollny, G. & Skinner, M. M. MIA-Clustering: a novel method for segmentation of paleontological material. *PeerJ* **6**, e4374 (2018).

[51] Dunmore, C. J., Kivell, T. L., Bardo, A. & Skinner, M. M. Metacarpal trabecular bone varies with distinct hand-positions used in hominid locomotion. *J. Anat.*, **235**, 45-66 (2019).

[52] Sukhdeo, S., Parsons, J., Niu, X. M., & Ryan, T. M.. Trabecular bone structure in the distal femur of humans, apes, and baboons. *Anat. Rec*. **303***,* 129-149 (2018).

[53] Ryan, T. M. & Shaw, C. N. Trabecular bone microstructure scales allometrically in the primate humerus and femur. *Proc R Soc Lond [Biol]* **280**, e20130172 (2013).

[54] Ruff, C. B. Long bone articular and diaphyseal structure in Old World monkeys and apes. I: locomotor effects. *Am. J. Phys. Anthropol.* **119**, 305-34 (2002).

Acknowledgements

We are grateful to I. Livne (Powell-Cotton Museum), A. vanHeteren, M. Hiermeier (Zoologische Staatssammlung München), C. Boesch, U. Schwarz (MPI-EVA), A. Ragni (NMNH); M. Teschler-Nicola and R. Muehl (Natural History Museum, Vienna), J. Moggi-Cecchi and S. Bortoluzzi (University of Florence), F. Mayer (Museum für Naturkunde - Leibniz Institute for Evolution and Biodiversity Science, Berlin), B. Großkopf (Johann-Friedrich-Blumenbach-Institut für Zoologie und Anthropologie der Georg-August-Universität Göttingen), R. Macchiarelli (Museo Nazionale Preistorico Etnografico "Luigi Pigorini"), B. Zipfel (University of Witwatersrand), E. Gilissen and W. Wendelen (Musée Royal de l'Afrique Centrale), V. Volpato (Senckenberg Museum of Frankfurt), Dani Nadel (University of Haifa), I. Herskovitz (Tel Aviv University) for access to specimens in their care. We also thank David Plotzki (MPI-EVA) and Keturah Smithson (Cambridge Biotomography Centre) for assistance in scanning these specimens, as well as Matthew Tocheri for assistance with landmarking software and Leoni Georgiou for discussions that enhanced this manuscript. This research was supported by European Research Council Starting Grant #336301, European Union's Horizon 2020 research and innovation programme (Grant agreement No. 819960), the Max Planck Society and the Fyssen Foundation.

Author Contributions

CJD, MMS and TLK conceived of and designed the study. CJD collected and analysed the data. AB and DHP contributed analysis tools. AR, J-JH, LRB, and NBS contributed data and theoretical context. CJD wrote the manuscript with input from all authors.

Competing interests

The authors declare no competing interests.

Data Availability

The data used to generate the analyses and graphs is now available at:
https://data.kent.ac.uk/id/eprint/111

Code Availability

All computational functions in the methods section are available in the software described in the Supplementary Information (S7).

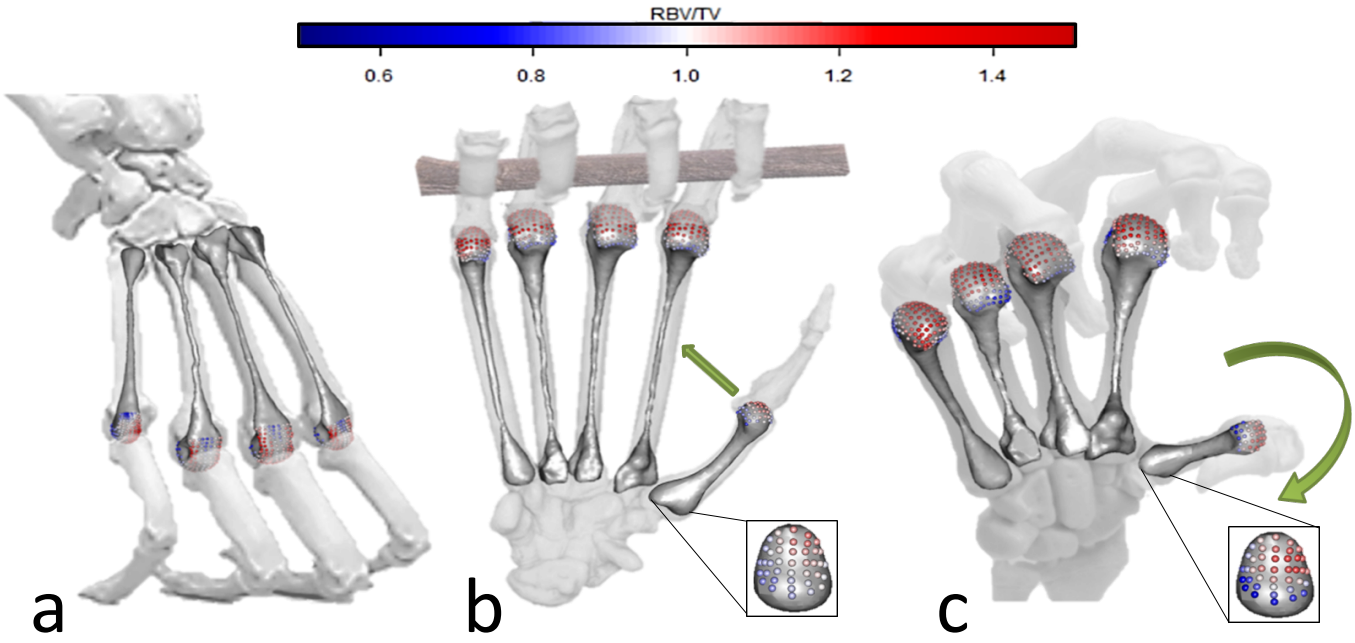
RBV/TV
0.6
0.8
1.0
1.2
1.4
a
b
c

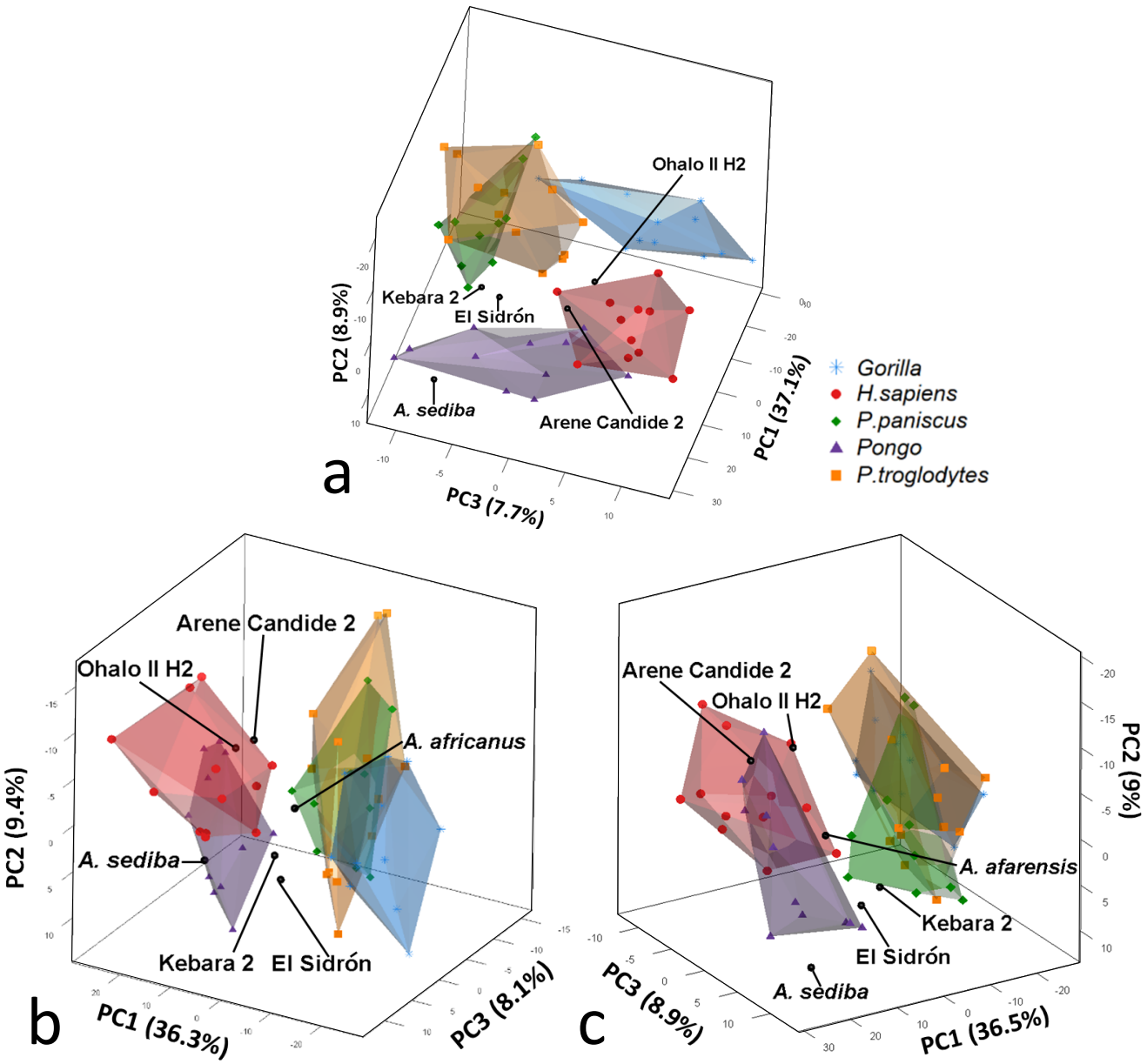
a
Ohalo II H2
Kebara 2
El Sidrón
A. sediba
Arene Candide 2
PC2 (8.9%)
PC1 (37.1%)
PC3 (7.7%)
Gorilla
H.sapiens
P.paniscus
Pongo
P.troglodytes
b
Arene Candide 2
Ohalo II H2
A. africanus
A. sediba
Kebara 2
El Sidrón
PC2 (9.4%)
PC1 (36.3%)
PC3 (8.1%)
c
Arene Candide 2
Ohalo II H2
A. afarensis
Kebara 2
El Sidrón
A. sediba
PC2 (9%)
PC3 (8.9%)
PC1 (36.5%)

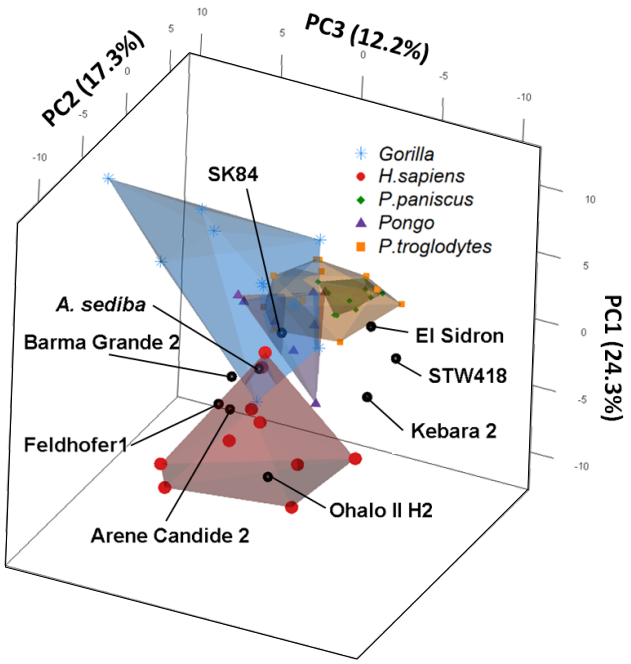
PC2 (17.3%)
PC3 (12.2%)
PC1 (24.3%)
Gorilla
H.sapiens
P.paniscus
Pongo
P.troglodytes
SK84
A. sediba
Barma Grande 2
Feldhofer1
Arene Candide 2
El Sidron
STW418
Kebara 2
Ohalo II H2

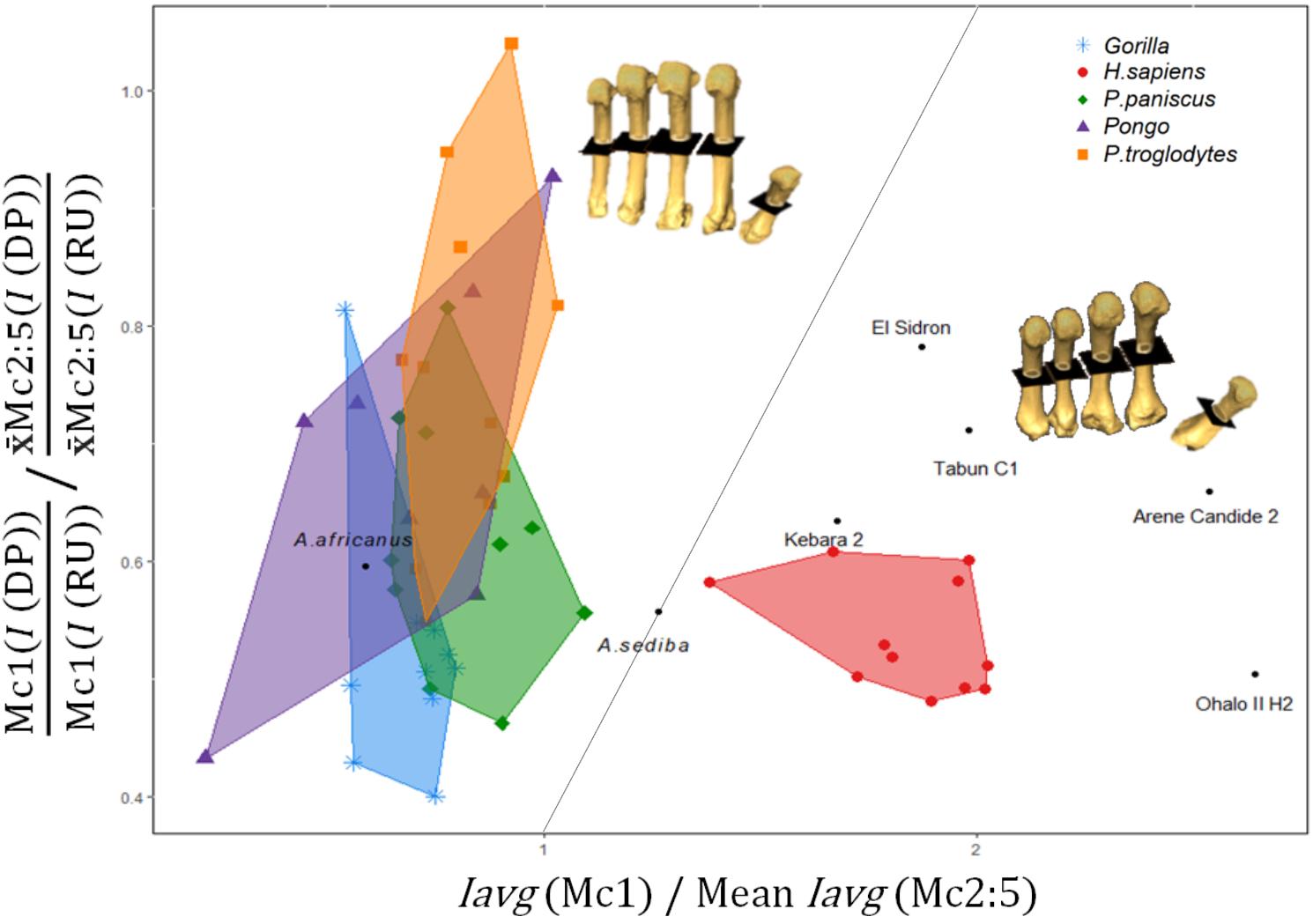
Gorilla
H.sapiens
P.paniscus
Pongo
P.troglodytes
El Sidron
Tabun C1
Arene Candide 2
Kebara 2
A.africanus
A.sediba
Ohalo II H2
1.0
0.8
0.6
0.4
1
2
$\frac{\mathrm{Mc1}(I\,(\mathrm{DP}))}{\mathrm{Mc1}(I\,(\mathrm{RU}))} / \frac{\bar{\mathrm{x}}\mathrm{Mc2{:}5}(I\,(\mathrm{DP}))}{\bar{\mathrm{x}}\mathrm{Mc2{:}5}(I\,(\mathrm{RU}))}$
Iavg (Mc1) / Mean *Iavg* (Mc2:5)

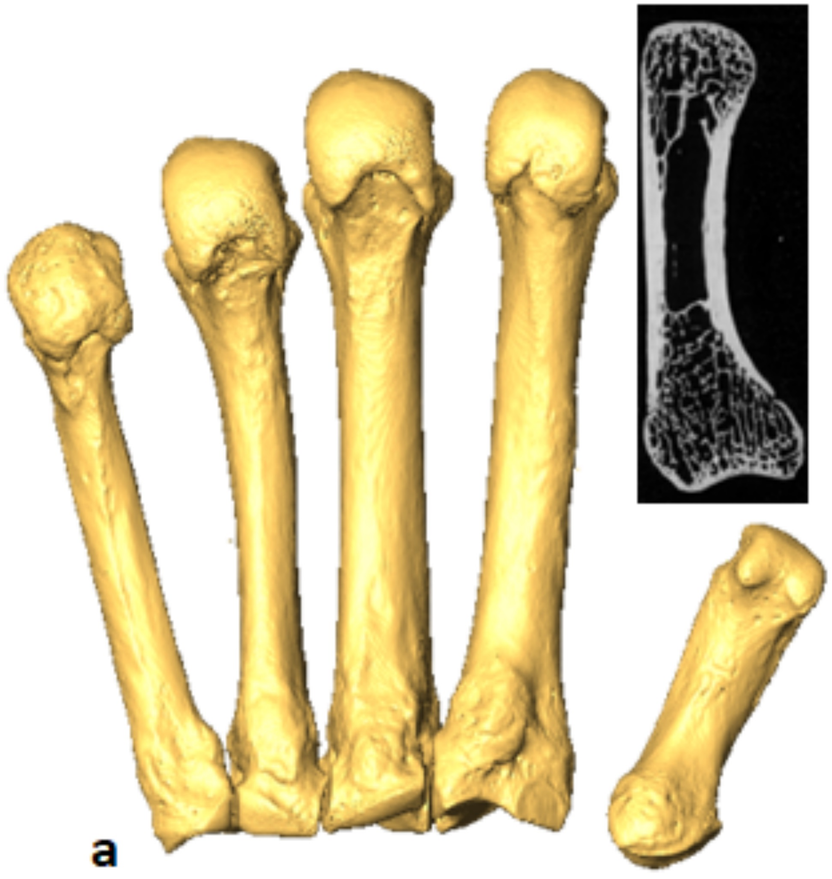

a

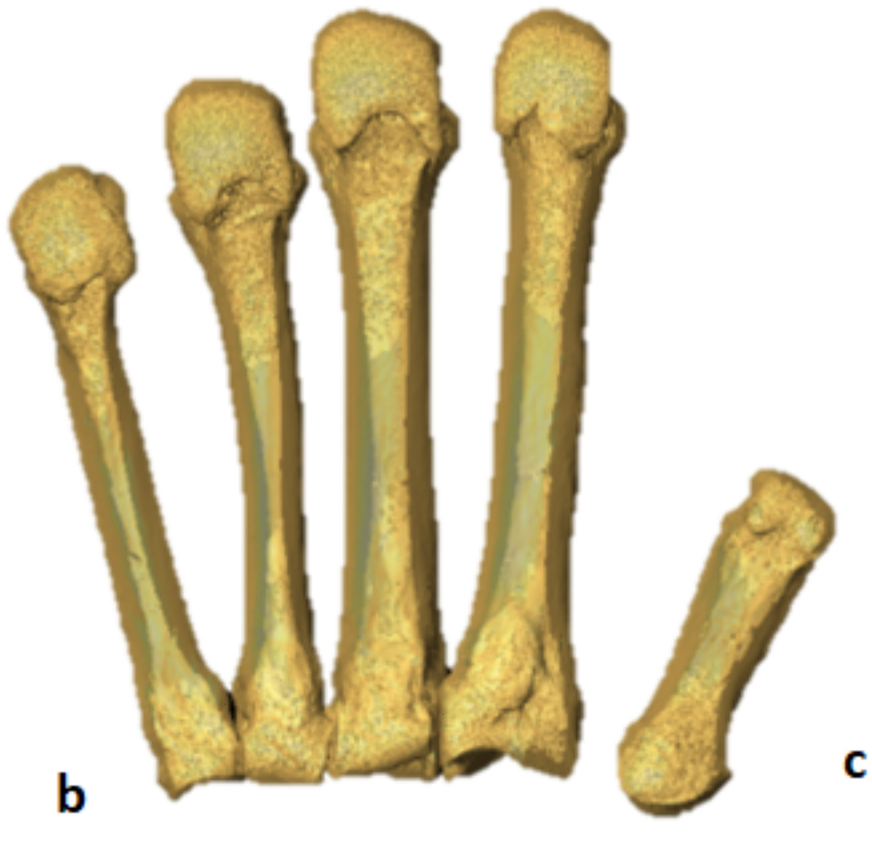

b

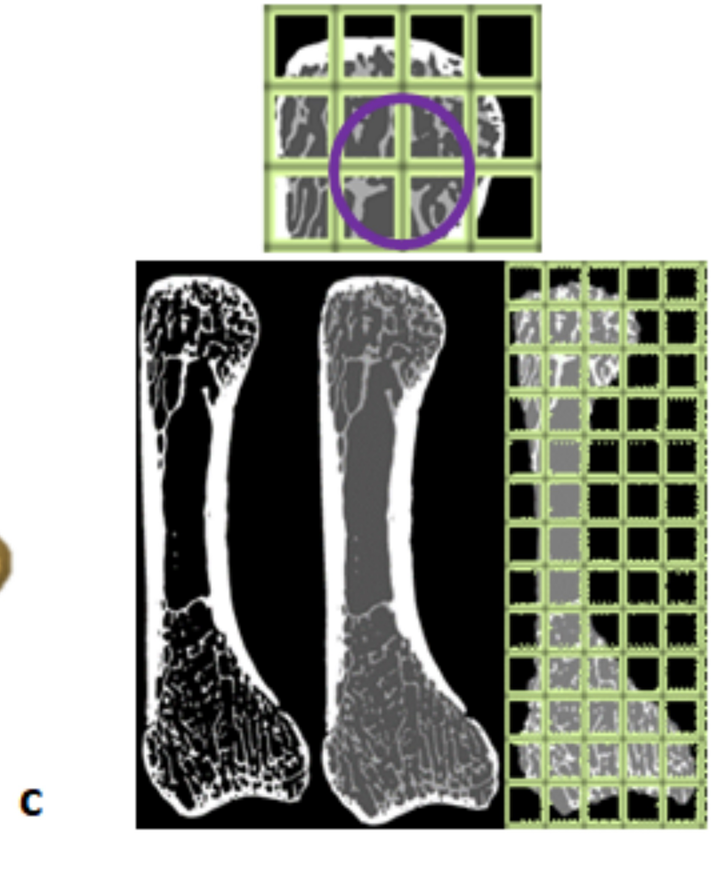

c

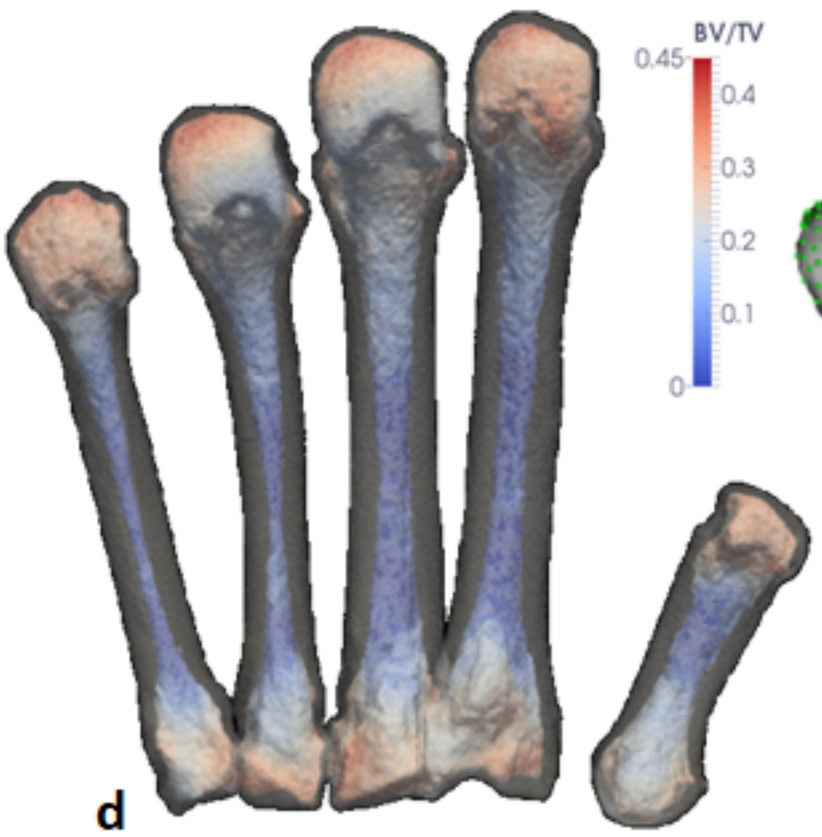

d

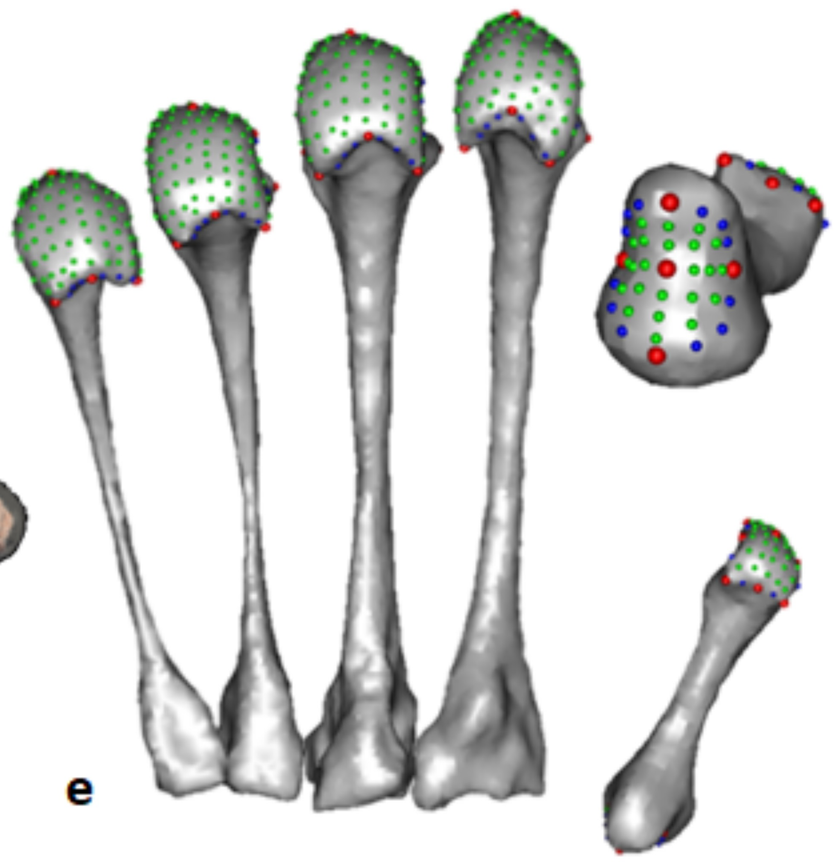

e

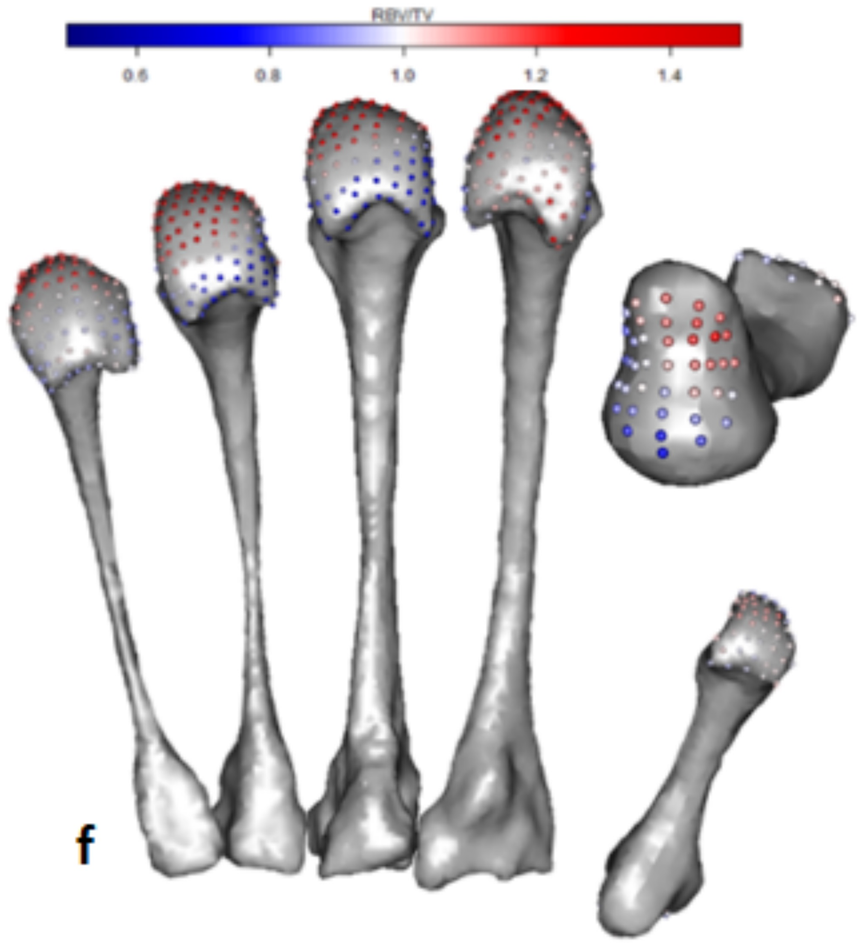

f

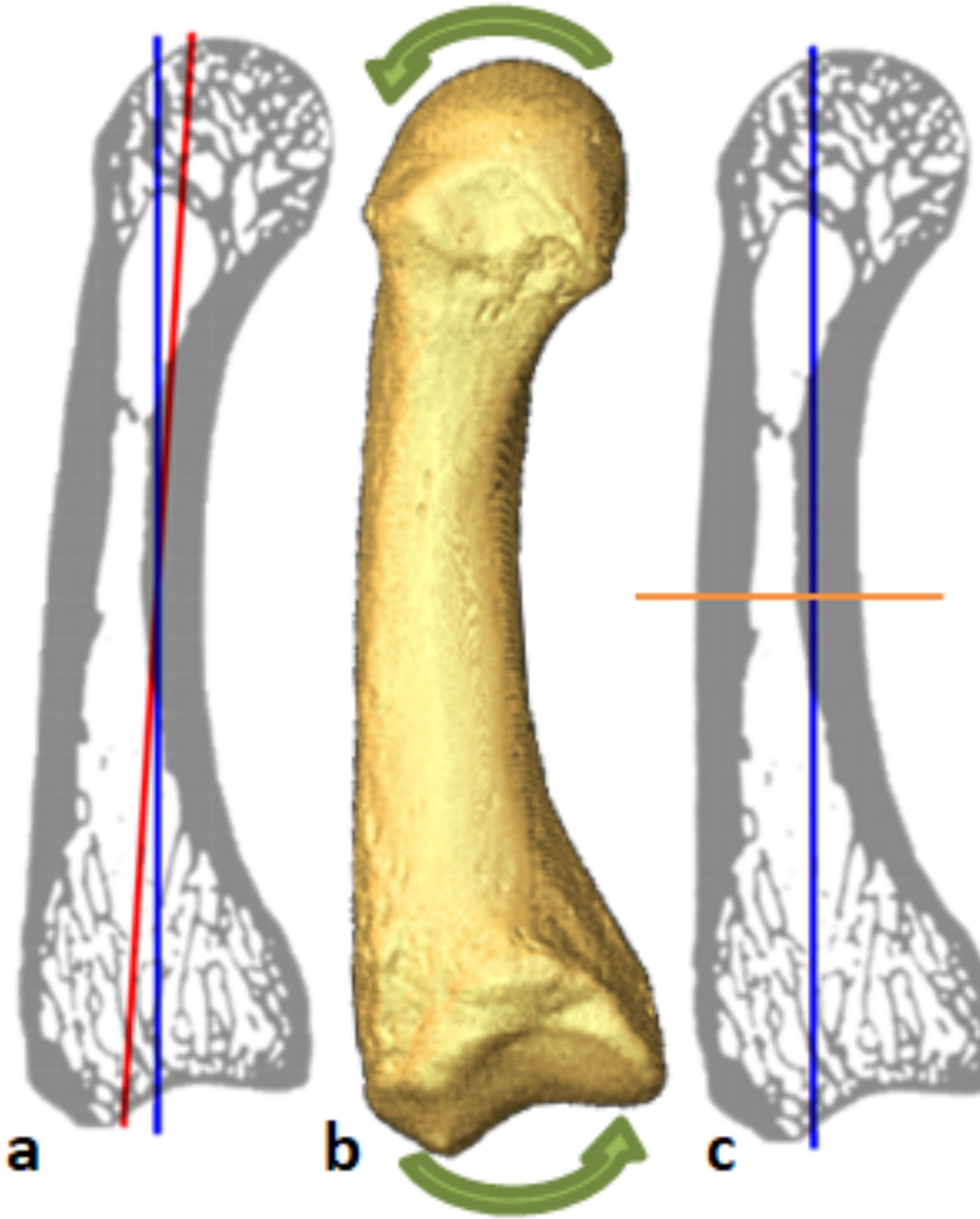
a
b
c


d

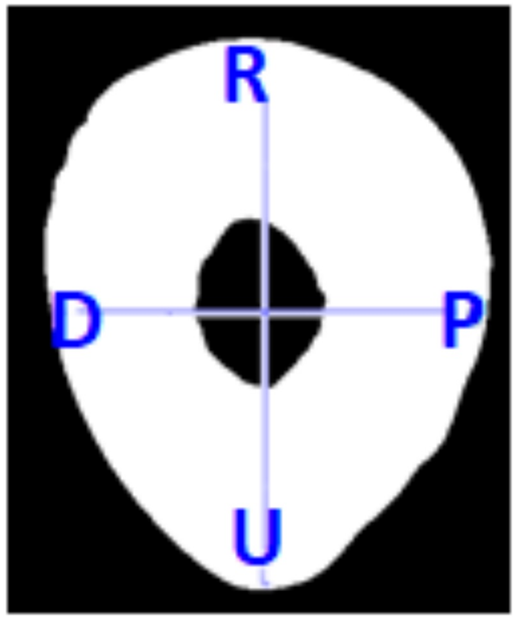
R
D
P
U
e

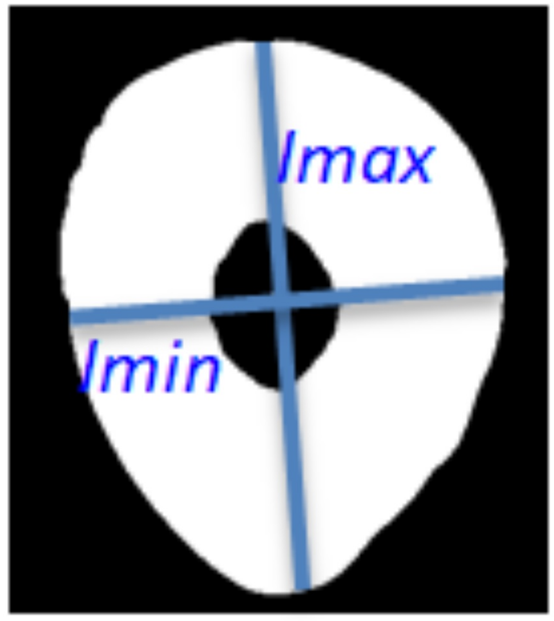
Imax
Imin
f

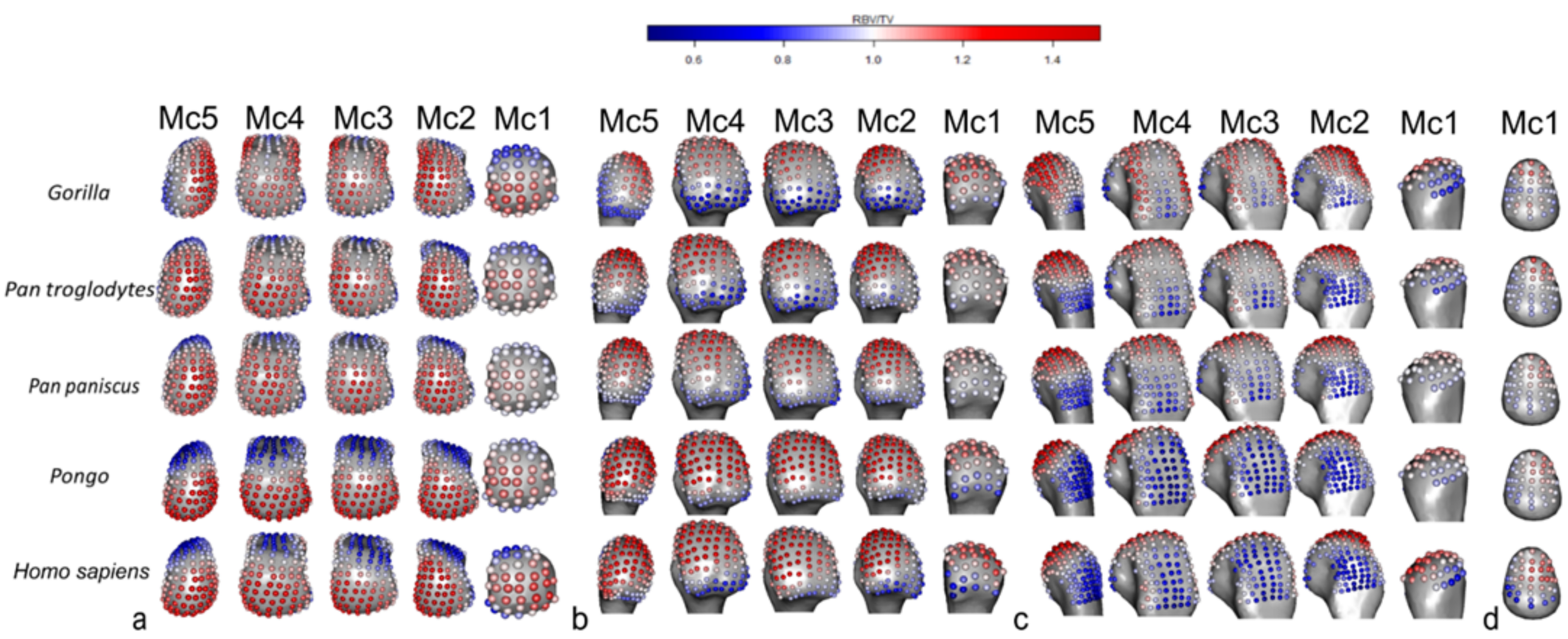
RBV/TV
0.6
0.8
1.0
1.2
1.4
Mc5
Mc4
Mc3
Mc2
Mc1
Gorilla
Pan troglodytes
Pan paniscus
Pongo
Homo sapiens
a
b
c
d

RBV/TV

0.6 0.8 1.0 1.2 1.4

Mc5 Mc4 Mc3 Mc2 Mc1 Mc5 Mc4 Mc3 Mc2 Mc1 Mc5 Mc4 Mc3 Mc2 Mc1 Mc1

Arene Candide 2

Ohalo 2 H2

Kebara 2

El Sidron

Au. sediba

Au. africanus

STW292 STW394 STW382 STW418 STW292 STW394 STW382 STW418 STW292 STW394 STW382 STW418 STW418

Au. afarensis

AL333-141 AL438-1d AL438-1e AL333-141 AL438-1d AL438-1e AL333-141 AL438-1d AL438-1e

a b c d

e

Feldhofer 1 Barma Grande 2 SK84